Article

Toward Pore Size-Selective Photoredox Catalysis Using Bifunctional Microporous 2D Triazine-Based Covalent Organic Frameworks

Melika Eshaghi Kenari,[#] Sayan Maiti,[#] Jianheng Ling, Xena El-Shamy, Hiren Bagga,
Matthew A. Addicoat, Phillip J. Milner, and Anindita Das*

Cite This: ACS Omega 2024, 9, 49249−49258

Read Online

ACCESS | Metrics & More | Article Recommendations | SI Supporting Information

ABSTRACT: The design and synthesis of photoactive metal-free 2D materials for selective heterogeneous photoredox catalysis continue to be challenging due to issues related to nonrecyclability, and limited photo- and chemical stability. Herein, we report the photocatalytic properties of a triazine-based porous COF, **TRIPTA**, which is found to be capable of facilitating both SET (single electron transfer) for photocatalytic reductive debromination of phenacyl bromide in absence of oxygen and generation of reactive oxygen species (ROS) for benzylamine photo-oxidation in the presence of oxygen, respectively, under visible light irradiation. Inspired by the latter results, we further systematically investigated different-sized benzyl-amine substrates in this single-component reaction and compared the results with an analogous COF (**Micro-COF-2**) exhibiting a larger pore size. We observed a marked improvement in the conversion of larger-sized substrates with the latter COF, thereby demonstrating angstrom-level pore size-selective photocatalytic activity of COFs.
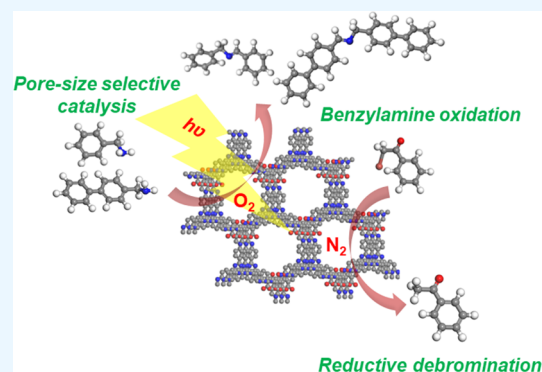
INTRODUCTION

Visible light-driven photoredox catalysis has received considerable attention in recent years on account of its ability to synthesize fine chemicals in an inherently straightforward, nontoxic, and sustainable manner. Over the years, several organic and transition metal complex-based photocatalysts have been reported.[1−8] However, significant drawbacks related to their stability, cost-effectiveness, and reusability limit their large-scale applications. To address these issues, heterogeneous photoactive solid catalysts such as TiO_2, graphitic carbon nitride, metal−organic frameworks (MOFs), and mesoporous silica,[9−13] are currently being explored. Despite showing promise as recyclable catalysts, these still suffer from issues such as fast charge recombination, low efficiency, exclusive operation in the UV region, high cost, and tedious separation methods. Additionally, the capability to tune reaction and substrate selectivity using many of these materials is rather limited. In this regard, low-cost, metal-free, robust covalent organic frameworks (COFs) present themselves as attractive materials to explore photocatalytic properties due to their layer-by-layer stacking architectures, ordered π-columnar channels, and 1-D pores.[14−18]

2D-COFs are a relatively new class of extended porous materials introduced by Yaghi and co-workers in 2005,[1] with low framework density and precise pores that can be easily customized with regard to both their chemical composition as well as network topology toward a wide range of desired applications. For the development of efficient COF-based heterogeneous photocatalysts, rational selection and precise assembly of photoactive building blocks into crystalline, extended porous frameworks is expected to enable charge separations, as well as the transportation and migration of photoinduced electron−hole pairs in photocatalytic reactions.[19−21] To this end, COFs incorporating organic moieties capable of affording single electron transfer (SET) as well as ROS generation under visible light irradiation are especially attractive since this chemistry is well-established for a variety of homogeneous and heterogeneous photocatalysts, including transition metal complexes, organic dyes, and inorganic semiconductors. In this regard, Liu and co-workers have recently reported a benzothiazole-based 2D-COF which photocatalyzes the dehalogenation of phenacyl bromide derivatives via an SET mechanism.[22] Meanwhile, several benzoxazole- and benzothiazole-based COFs have been recently reported that can catalyze the oxidation of amines and sulfides via ROS generation pathways.[23,24]
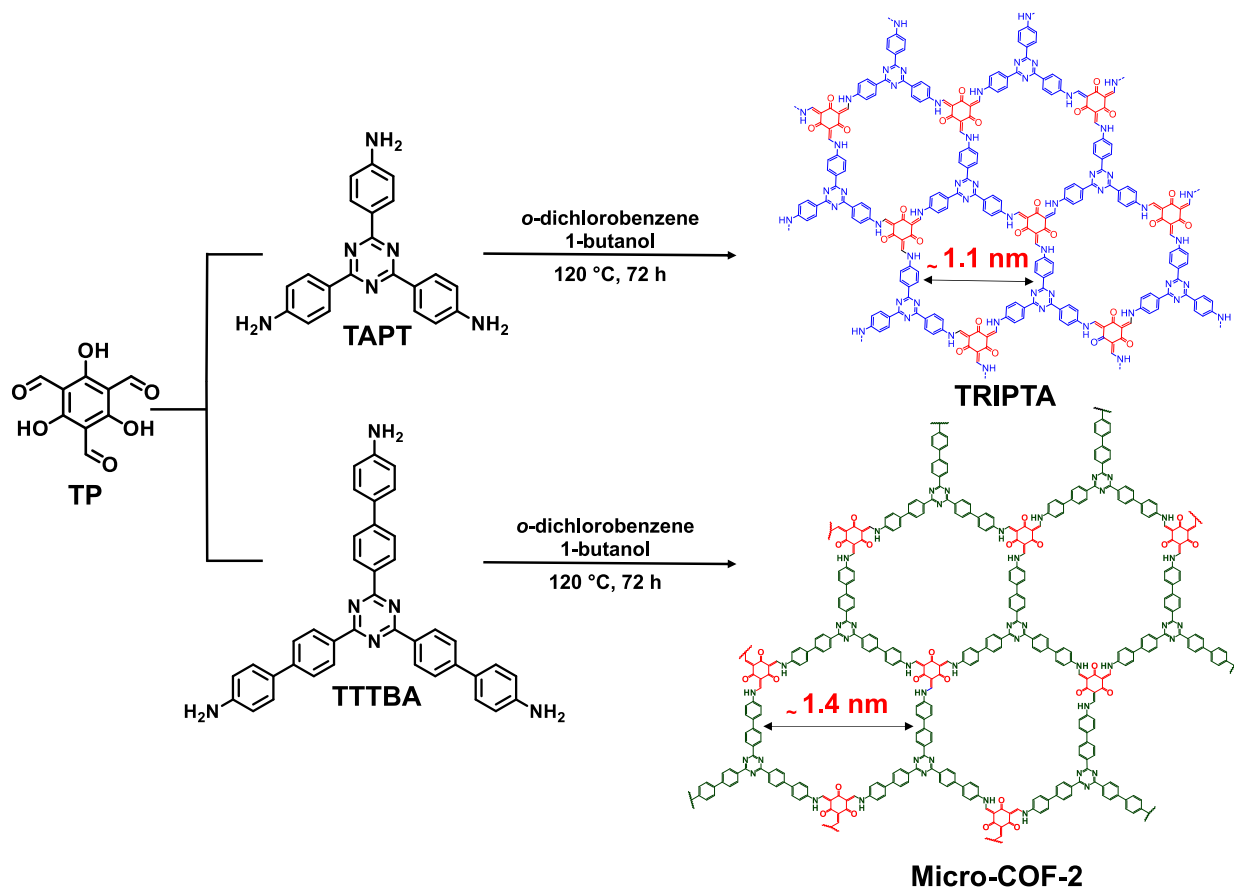
Scheme 1. Synthetic Scheme of TRIPTA and Micro-COF-2

Apart from the precise assembly of donor−acceptor moieties in the crystalline frameworks, the high porosity and surface area of porous materials have been correlated to higher photocatalytic activity.[25−28] For instance, the controllable modification of pore size in a variety of porous materials has been shown to enable precise tuning of substrate selectivity, thereby enhancing the selectivity of the chosen catalytic reaction.[29−31] With respect to 2D-COFs, Gao et al.[32] have recently demonstrated angstrom-level pore size selectivity in a series of COF-based membranes with different surface charge distributions toward the separation of water-soluble ionic liquids. Additionally, both pore volume and pore size have been shown to be critical for enhanced volatile iodine adsorption.[33] However, to the best of our knowledge, engineering angstrom-level, pore size-dependent substrate selectivity for photocatalytic reactions has not been broadly explored using 2D-COFs.

Considering the above-mentioned design requirements of an ideal COF-based photocatalyst, herein we chose to investigate the photocatalytic properties of a previously reported micro-porous 2D-COF, **TRIPTA**[34] (Scheme 1). This COF, belonging to a well-known class of β-keto enamine COFs[35,36] was specifically chosen as a model material to explore photocatalytic properties due to a combination of factors including (1) the planar structure of the triazine-based, amine-monomer is expected to enhance π interactions between the COF layers to improve its crystallinity and hence, serve as a π stabilizer;[20] (2) the presence of donor−acceptor moieties in the COF framework should enable improved charge separation, thereby leading to significantly improved photo-

catalytic activity; and finally, (3) introduction of 2,4,6-triformylphloroglucinol as the aldehyde-monomer with an electron-rich group should enhance the chemical stability of the COF skeleton through resonance effects and improve triplet state stabilization.[20]

TRIPTA was found to photocatalyze two different model reactions, namely (1) photocatalytic reductive debromination reactions of phenacyl bromides via C−Br bond cleavage under N_2 atmosphere via an SET pathway, and (2) photocatalytic self-coupling reactions of aromatic benzylamines derivatives via ROS generation, highlighting its potential to facilitate multiple photoinduced pathways. Interestingly, the second model reaction yielded poor photocatalytic conversion rates for larger-sized benzylamine substrates under identical reaction conditions. Utilizing an analogous **Micro-COF-2**,[33] with a bigger pore size than **TRIPTA** (Scheme 1) led to dramatically improved photocatalytic conversion (>95%) for the larger-sized benzylamine derivatives. Taken together, our findings suggest that porous triazine-based 2D-COFs could be an emerging class of pore size- and shape-selective catalysts for various organic reactions.

■ EXPERIMENTAL SECTION

Materials. 4-Aminobenzonitrile, phloroglucinol, triflic acid, trifluoroacetic acid, hexamethylenetetramine (HMT), chloroform, 1,4-dioxane, o-dichlorobenzene, dimethyl sulfoxide (DMSO), N,N-dimethyl acetamide, hydrochloric acid and all the relevant solvents were acquired from Sigma-Aldrich, Alfa Aesar, and Thermo Fisher and used without additional purification unless otherwise noted.
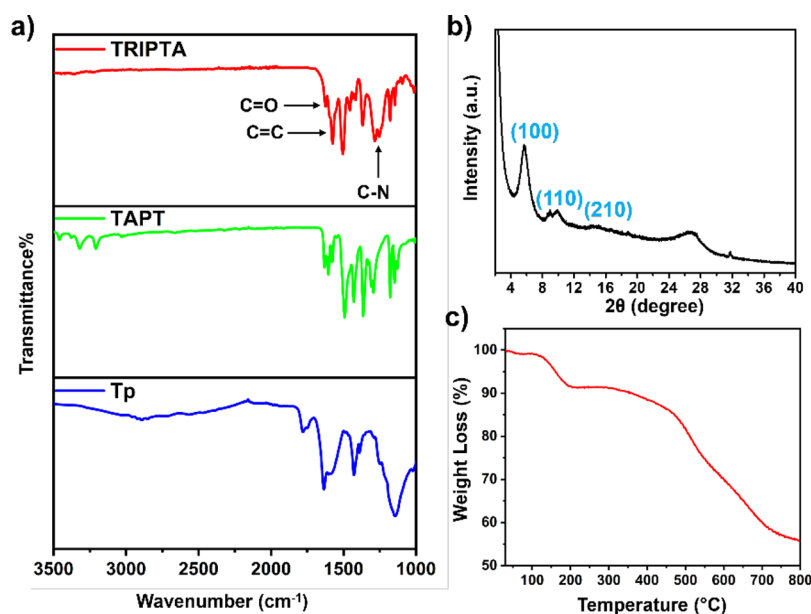
Figure 1. Characterization of **TRIPTA**. (a) FT-IR spectra depicting the signature stretching frequencies in comparison with the starting materials (TAPT and TP); (b) Powder XRD pattern confirming its crystallinity; (c) TGA curve demonstrating the high thermal stability.

Methods. The covalent organic frameworks in this study were analyzed using Brunauer−Emmett−Teller (BET), PXRD, Solid-state UV−vis, Fourier-transform infrared spectroscopy (FT-IR), Solid-state NMR, Thermogravimetric analysis (TGA), and Scanning Electron Microscopy (SEM). Additional details are provided in the Supporting Information.

Synthetic Procedures for TAPT, TP, and TTTBA. 1,3,5-tris(4-aminophenyl)triazine (TAPT)[43] was synthesized by reacting 4-aminobenzonitrile (350 mg, 2.96 mmol) with trifluoromethanesulfonic acid (CF$_3$SO$_3$H, 1.5 mL) in 25 mL chloroform (CHCl$_3$) overnight at 0 °C under argon. Quenching of the reaction mixture by ice-cold water and neutralization using aqueous 2 N NaOH, yielded TAPT as a beige powder after washing steps (see Section S2, Supporting Information). The preparation of 1,3,5-Triformylphloroglucinol (Tp)[42] was carried out by reacting hexamethylenetetramine (2.5 g, 17.83 mmol) and phloroglucinol (1 g, 7.92 mmol) in 25 mL of trifluoroacetic acid (TFA) at 100 °C for 5 h under argon atmosphere. The reaction mixture was stirred, quenched with 3 N hydrochloric acid, and heated further at 100−110 °C for 1.5 h. After cooling to RT, extraction with DCM, rotary evaporation of the organic layers and washing with EtOH gave the final product (see Section S3, Supporting Information). 4,4′,4″-(1,3,5-triazine-2,4,6-triyl) tris([1,1′-biphenyl]-4-amine) (TTTBA) was prepared by treating 4-(4-aminophenyl)benzonitrile (0.25 g, 1.28 mmol) with CF$_3$SO$_3$H (300 μL) overnight at 0 °C under argon atmosphere. Quenching with ice-cold water, followed by neutralization with 2 N NaOH and subsequent washing of the precipitate gave the final product (see Section S4, Supporting Information).

Synthetic Procedure of TRIPTA and Micro-COF-2. **TRIPTA** was constructed via a solvothermal condensation reaction. 60 mg TAPT (0.17 mmol) and 35 mg Tp (0.16 mmol) were placed in a Pyrex tube, followed by a stepwise addition of 1 mL *n*-butanol, 1 mL *o*-dichlorobenzene and 0.2 mL 6 M acetic acid. The reaction mixture was sonicated for 30−35 min to make a homogeneous ink-type dispersion. **Micro-COF-2** was constructed using the same solvothermal

condensation process as described above for **TRIPTA**, using 60 mg TTTBA (0.102 mmol), 20 mg Tp (0.102 mmol), 1 mL *n*-butanol, 1 mL *o*-dichlorobenzene and 0.5 mL 6 M acetic acid (see Sections S5 and S6, Supporting Information).

■ RESULTS AND DISCUSSION

The synthesis of two triazine-based COFs, **TRIPTA** and **Micro-COF-2** were carried out according to previously reported procedures.[33,34] Briefly, both COFs were synthesized using Schiff base condensation reactions between 2,4,6-triformylphloroglucinol (TP, aldehyde-monomer) and either a triazine-based amine-monomer 1,3,5-tris(4-aminophenyl)-triazine (TAPT) in the case of **TRIPTA**, or an extra phenyl group-containing 4,4′,4″-(1,3,5-triazine-2,4,6-triyl) tris([1,1′-biphenyl]-4-amine) (TTTBA) in the case of **Micro-COF-2**, as shown in Scheme 1. The COFs were characterized by Fourier-transform infrared spectroscopy (FT-IR), ^{13}C cross-polarized/magic angle spinning solid-state nuclear magnetic resonance (^{13}C CP-MAS ssNMR), thermogravimetric analysis (TGA), solid-state UV/vis, Brunauer−Emmett−Teller analysis (BET), powder X-ray diffraction (PXRD) and scanning electron microscopy (SEM). Starting with **TRIPTA,** we first performed FT-IR to confirm the chemical composition and free functionalities within the COF framework (Figure 1a). Stretching bands at 1623, 1575, and 1256 cm^{-1} can be assigned to −C=O, −C=C, and −C−N functionalities, respectively, establishing the presence of β-keto enamine linkages. The crystallinity of **TRIPTA** was confirmed using wide-angle powder X-ray diffraction (PXRD, Figure 1b). The diffraction peaks (2θ) at 5.8, 10.0, and 15.6 indicate the presence of 100, 110, and 210 planes, respectively. Additionally, a broad peak at 26.19 illustrates strong π···π stacking interactions between the layers of **TRIPTA**.[34,37,38] The small peak at 32° could be attributed to noise. Simulations (Figures S1 and S2) show good agreement with the experimental data, and depict regular slip stacked structures (both AA and AB stacking mode).
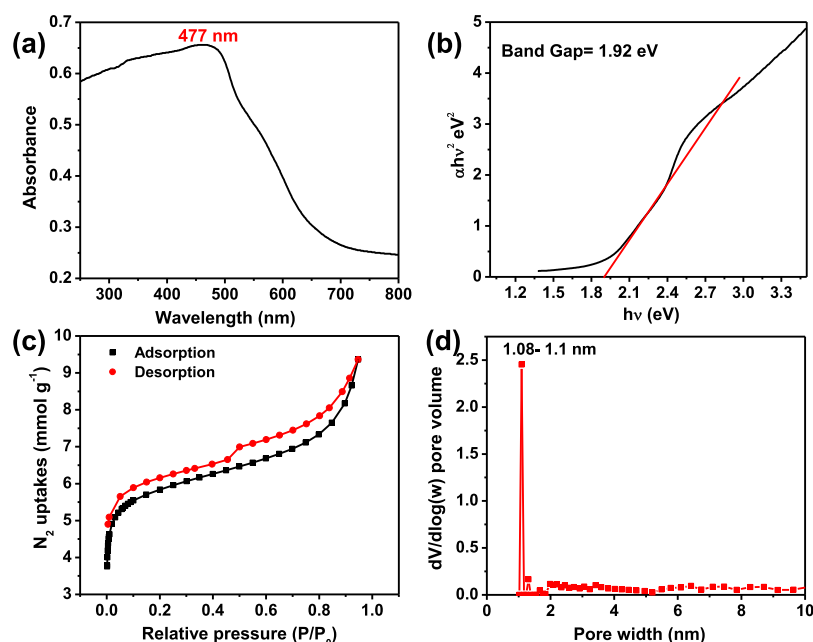
Figure 2. Characterization results of **TRIPTA** (a) Solid-state UV−visible spectrum depicting the signature $\pi-\pi^*$ transition. (b) Band gap determination via the Tauc plot. (c) N_2 gas adsorption−desorption isotherm (77 K). (d) Pore size distribution evaluation (NLDFT), yielding a calculated pore size of ∼1.1 nm.

To examine the thermal stability of **TRIPTA**, thermogravimetric analysis (TGA) was performed (Figure 1c). The TGA curve reveals an initial weight loss of approximately 1.64%, which can be attributed to the residual dissociation of water molecules from the pores. Subsequently, a weight loss of 7.23% was observed within the temperature range of 130 to 200 °C, indicating the evaporation of residual solvents that were trapped inside pores (Figure S3). Furthermore, a weight loss of 4.18% in the temperature range of 200 to 427 °C, can be attributed to the degradation of the framework. Finally, a significant weight loss of 31.64% is observed within the temperature range of 427 to 800 °C. Overall, the TGA analysis unequivocally establishes the exceptional thermal stability of **TRIPTA**. Cross-polarized magic angle spinning (CP-MAS) solid state ^{13}C NMR provided additional support for the structure (Figure S4), revealing the chemical environment for each type of carbon atom present in the **TRIPTA** framework. The carbon atom in the enamine was observed at 146 ppm, which is a signature peak for successful **TRIPTA** formation. The surface morphology was then investigated using SEM, revealing the presence of relatively small crystallite particles on the surface (Figure S5).

The solid-state UV−vis absorption spectrum of **TRIPTA** shows absorbance maxima at 477 nm, which can be attributed to the $\pi-\pi^*$ transition (Figure 2a). Furthermore, the band gap was determined to be 1.92 eV through Tauc plot analysis (Figure 2b). To investigate the surface area and pore size distribution, BET (Brunauer−Emmett−Teller) surface area analysis was performed using N_2 adsorption analysis at 77 K and 1 bar pressure. The maximum N_2 uptake was found to be 9.36 mmol g^{-1} (Figure 2c), and the BET surface area was calculated to be 430 m^2 g^{-1}. **TRIPTA** adsorbs significant amounts of N_2 at lower pressures (0−0.1 bar), indicating the presence of microporosity in the framework. Consistently, the pore size distribution was evaluated using the nonlocal density functional theory (NLDFT) model, yielding a calculated pore size of ∼1.1 nm (Figure 2d). ^1H NMR spectra of the

monomers TAPT and Tp have been provided in the Supporting Information (Figures S6 and S7, respectively), while characterization details of the analogous **Micro-COF-2** are depicted by Figures S8, S9, and S10.

Photocatalytic Reductive Debromination Using TRIPTA. Given its band gap of 1.92 eV, we hypothesized that **TRIPTA** could be utilized as a photocatalyst for organic transformations.[39,40] COFs with similar band gaps have been demonstrated to carry out photocatalytic dehalogenation of phenacyl bromides,[39] indicating the thermodynamic feasibility of the process. To investigate its photocatalytic properties, we chose a well-studied model reaction involving dehalogenation of phenacyl bromide under blue light irradiation in the presence of 1,4-dihydropyridine dicarboxylate (Hantzsch ester) and *N,N*-diisopropyl ethylamine (DIPEA) under N_2 atmosphere (Table 1, entry 1). This reaction is known to proceed via the single electron transfer (SET) pathway, wherein DIPEA and Hantzsch esters serve as sacrificial agents by donating electrons and protons, respectively.[40−44] Gratifyingly, using **TRIPTA** as a photocatalyst, excellent conversion up to ∼88% to the acetophenone product can be achieved as determined by ^1H NMR analysis (see Figures S11−S14) This catalytic performance was found to be comparable to (and in some cases superior to) other reported photocatalysts (Table S1). To further explore the substrate scope of these reactions, we included phenacyl bromide derivatives with either electron-donating or electron-withdrawing groups. As depicted in Table 1 (Entries 2−5), **TRIPTA** catalyzes the photoreductive debromination of various phenacyl bromide derivatives into their respective acetophenones with quite high conversion rates (70−98%). Hence, significant correlations between the conversion rates and the electronic effects of substitutions could not be ascertained.

To evaluate the photocatalytic efficiency of **TRIPTA** compared to its building blocks, we conducted control experiments with TP and TAPT under identical conditions. We observed that only **TRIPTA**, not its monomers

Table 1. Substrate Scope of TRIPTA-Catalyzed Photoreductive Dehalogenation of Phenacyl Bromides[A]

Entry	Substrate	Product	Time (h)	Conversion (%)
1			12	88
2	(OMe)	(OMe)	12	91
3	(Me)	(Me)	12	82
4	(Br)	(Br)	12	70
5	(Cl)	(Cl)	12	98

[A]Reaction conditions: 0.17 mmol of α-bromoacetophenone derivatives, DIPEA (0.34 mmol, 60 μL), Hantzsch ester (0.17 mmol, 44 mg) in 2 mL N,N-dimethylformamide solvent and 10 wt % of TRIPTA, stirring under blue light at room temperature under nitrogen atmosphere for 12 h.

demonstrated catalytic activity (Figures S15 and S16). As seen in previous studies, we observed an inert atmosphere is essential for obtaining high conversions for this reaction.[40] Hence, we hypothesize that this reaction proceeds via the formation of radical species under photoreductive conditions (Scheme 2).[40] Specifically, when irradiated with blue light, TRIPTA is proposed to act as an efficient photosensitizer, giving rise to the excited [TRIPTA]* species. This is followed by the oxidation of Hantzsch ester, producing free-radical cations via electron donation to [TRIPTA]*. The resulting

Scheme 2. Proposed Mechanism of the Photoreduction Dehalogenation Reaction Using TRIPTA as a Photocatalyst
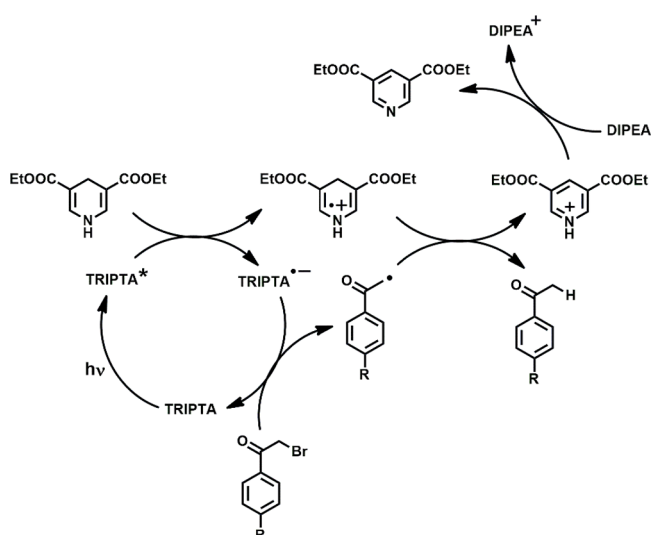
radical anion [TRIPTA]•− drives the dehalogenation of α-bromoacetophenone via the single electron transfer (SET) pathway, returning TRIPTA to its ground state and forming the intermediate phenone radical. This intermediate abstracts an H atom from the radical cation of Hantzsch ester, leading to the generation of the final product. Finally, the protonated pyridine Hantzsch ester is neutralized by DIPEA, completing the catalytic cycle.

Encouraged by the ability of TRIPTA to facilitate SET in the photoreductive debromination reaction, we wanted to investigate if it was also capable of promoting generation of ROS under ambient reaction conditions. Hence, we decided to test TRIPTA as a photocatalyst for the oxidative self-coupling of benzylamine, a model reaction that is known to proceed via ROS generation wherein air acts as an oxygen source.[45−52] We observed a conversion of ∼99% within 1 h (determined by ^{1}H NMR analysis, see Figures 3a and S17), highlighting the photocatalytic efficiency of TRIPTA. Control studies using TAPT, TP, or no catalyst yielded negligible conversions (Figure 3a). The amount of photocatalyst was then varied to investigate its impact on conversion (Figure 3b). A gradual increase in conversion rates was observed with increasing wt % of the catalyst, with a maximum conversion of over 95% for 10 wt % catalyst loading.

The recyclability of TRIPTA as a heterogeneous photocatalyst was examined (Figure 3c and Section S8), and we observed that TRIPTA acts as an efficient photocatalyst up to four cycles, although the conversion is found to be reduced to ∼50% (Figure S18). To understand the cause of reduction in conversion, we performed PXRD on recycled TRIPTA (after fourth catalytic cycle) which shows some loss of crystallinity in TRIPTA (Figure S19). This along with some degree of pore-blocking due to incomplete removal of products during the washing steps is hence ascribed to be the source of reduction in photocatalytic activity of TRIPTA in each recycling step. We also carried out FT-IR analysis on the recovered TRIPTA (after 1 cycle), which revealed no major change in the frequency patterns (Figure S20), demonstrating the overall stability of the COF. Further, kinetic studies were performed which confirmed the optimal reaction time to be 1 h (Figure 3d). To confirm the role of oxygen in determining the outcome of the reaction, we conducted the reaction under N_2 atmosphere. Under these inert conditions, we did not observe any significant conversion of benzylamine to its oxidative products which confirms the major key role of ROS in the reaction mechanism.

To gain insights into the molecular pathways involved in the blue-light-driven oxidation of the benzylamine, we investigated the impact of 2,2,6,6-tetramethylpiperidine 1-oxyl (TEMPO, as a reactive oxygen species scavenger), silver nitrate (AgNO$_3$, as an electron scavenger), and potassium iodide (KI, as a hole scavenger) on the reaction (Figures S21−S23). A reduction in the conversion of benzylamine to the self-coupled product was observed in the presence of each of these reagents. These results highlight the roles of the photogenerated ROS ($^1O_2$ and/or $O_2^{•−}$), electrons, and holes in the overall catalytic process. Based on these results and prior literature reports,[45−52] we propose a plausible mechanism for the selective oxidative of benzylamine, with $O_2^{•−}$ as the ROS (Scheme 3). TRIPTA, the photocatalyst employed, generates electron−hole pairs under blue light irradiation. The photogenerated electrons interact with O_2 to form $O_2^{•−}$. Simultaneously, benzylamine is oxidized by the holes (h$^+$) to
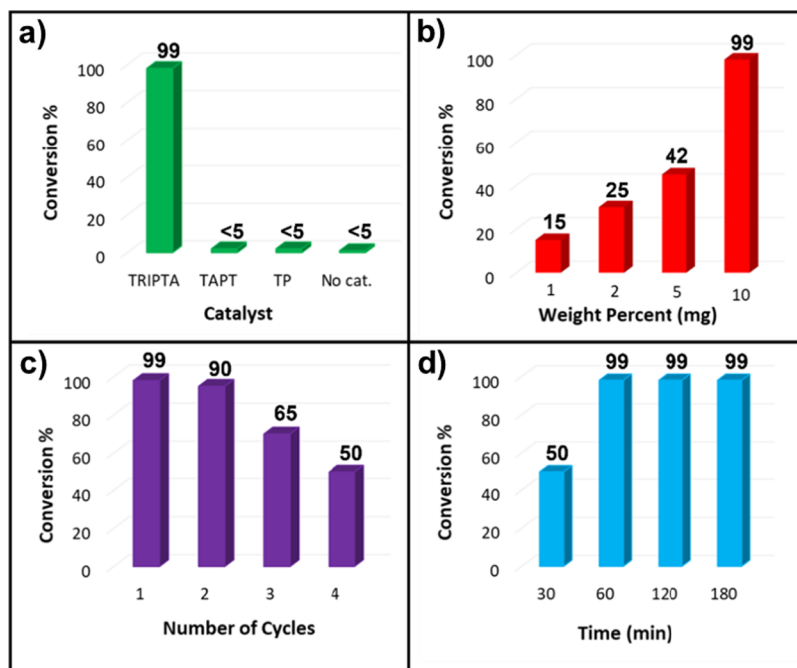
Figure 3. Photooxidation reaction using **TRIPTA** as the photocatalyst and benzylamine as the substrate: a) comparison of the photocatalytic performance of **TRIPTA** and its building blocks in the photooxidation reaction; b) optimized weight percent of the catalyst; c) recyclability of the heterogeneous catalyst after four cycles; d) kinetic study depicting the maximum yield obtained after 1 h. **Reaction conditions**: 0.33 mmol of benzylamine derivatives in 2 mL of acetonitrile and 10 wt % **TRIPTA** were stirred under blue light at room temperature.

Scheme 3. Proposed Mechanism for the Photooxidation Reaction of Benzylamine Using TRIPTA as the Photocatalyst
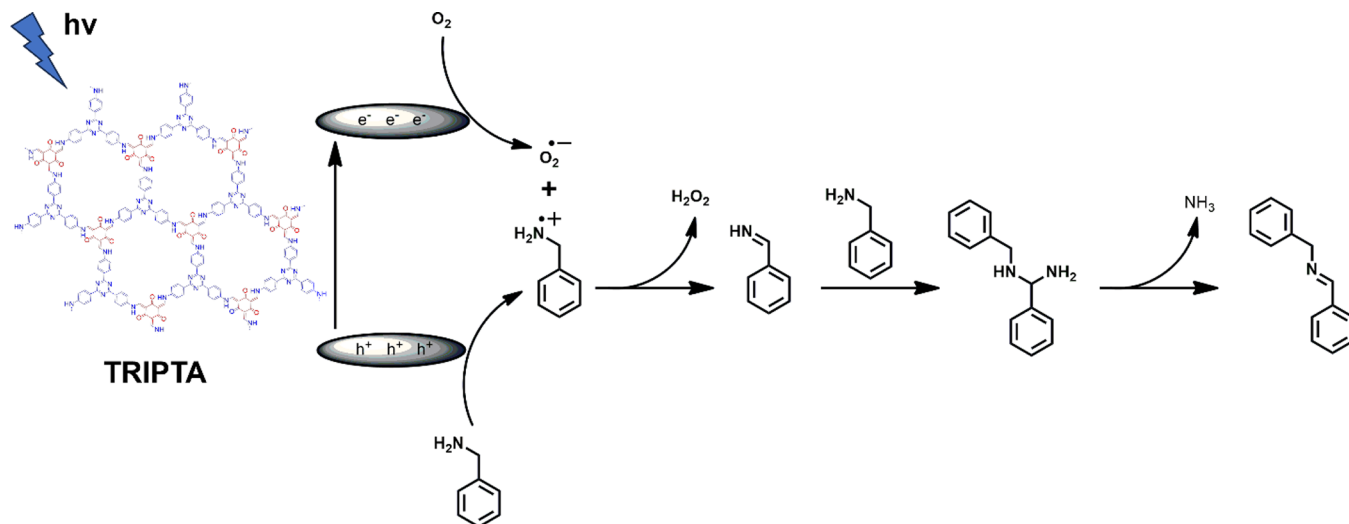
produce the benzylamine radical cation. Subsequently, the $O_2^{\bullet-}$ abstracts a hydrogen atom from the benzylamine amine to form the radical cation intermediate, imine, and H_2O_2. Finally, the desired product molecule of N-benzylidenebenzyl-amine, is formed through the coupling of imine intermediate with benzylamine.

Pore Size Selective Photocatalytic Performance of TRIPTA and Micro-COF-2. To explore the substrate scope, we expanded our study to include a wide range of benzylamine substrates, including those substituted with para-substituents R = −Me, −OMe, −Br, −Cl, −F, −I. **TRIPTA** was found to efficiently catalyze the self-coupling reactions, exhibiting conversion rates of greater than 95% (Table 2 and Figures S24−S27). Further, we investigated the same photocatalytic

reaction using larger benzylamine derivatives such as 4-phenylbenzylamine and 4-(4-fluorophenyl)benzylamine (Table 3). Surprisingly, efficient photocatalytic activity was not observed using these substrates (Figures S28 and S29). Moreover, changing the reaction solvent did not affect the conversion rates. These observations led us to speculate that **TRIPTA** could be size-selective toward smaller benzylamines in these oxidation reactions. We measured the approximate dimensions of benzylamine derivatives using Material Studio 7.0 software (Table S2). Notably, we observed that all the benzylamine substrates, except for 4-phenylbenzylamine and 4-(4-fluorophenyl)benzylamine, fit within the micropores (~11 Å) of the **TRIPTA**. Based on this finding, we proposed that the reaction occurs within the confined space of the microporous,

Table 2. Selective Photocatalytic Oxidative Self-coupling of Substituted Benzylamines Using TRIPTA under Blue Light Irradiation and Air[A]

Entry	Substrate	Product	Time (h)	Conversion (%)
1	(4-H benzylamine)	(imine product)	1	99
2	(4-I benzylamine)	(imine product)	1	95
3	(4-F benzylamine)	(imine product)	1	96
4	(4-Br benzylamine)	(imine product)	1	95
5	(4-Cl benzylamine)	(imine product)	1	96
6	(4-Me benzylamine)	(imine product)	1	98
7	(4-OMe benzylamine)	(imine product)	1	96

[A]**Reaction conditions**: 0.33 mmol of benzylamine derivatives in 2 mL of acetonitrile and 10 wt % **TRIPTA** were stirred under blue light at room temperature for 1 h.

where size-selective photocatalytic oxidation of benzylamines occurs. And since **TRIPTA** does not demonstrate sufficient catalytic activity for the larger benzylamines, it can be inferred that its pore size or shape prevents effective interaction with the photocatalyst.

To substantiate our assumptions, we utilized the structurally analogous **Micro-COF-2** as the photocatalyst since it exhibits a larger average pore size (1.4−1.5 nm) in comparison to

TRIPTA. We observed a noticeable conversion, exceeding 80% for the oxidation of 4-(4-fluorophenyl)benzylamine and 4-phenylbenzylamine in the presence of **Micro-COF-2** as the photocatalyst (Figures S30 and S31). This clearly demonstrates that the larger micropore size of **Micro-COF-2** could better accommodate the larger-sized benzylamine derivatives, resulting in greater photocatalytic conversions. This, in turn, proves that the photocatalytic activity of 2D-COFs can be tuned at the angstrom-level by rationally controlling their pore sizes. To further confirm the pore size-selective photocatalytic behavior of COFs, we investigated the impact of pore-clogging in **TRIPTA** on its photocatalytic activity. Initially, we blocked **TRIPTA**'s pores using *meta*-xylene as a clogging agent. Subsequent analyses of BET surface area and pore size indicate a noteworthy reduction in pore size to ultramicropores (0.7 nm) in the resulting material (Figure S32), termed meta-xylene@TRIPTA. Following this modification, we investigated the photocatalytic performance of meta-xylene@TRIPTA in a benzylamine coupling reaction. Notably, the results revealed a modest 17% conversion to the product, highlighting the selective nature of our pore size-dependent photocatalysis (Figure S33). This observation emphasizes the significance of comprehending pore characteristics in photocatalytic processes and offers valuable insights into potential applications of **TRIPTA** and **Micro-COF-2** in selective catalytic transformations.

■ CONCLUSION

In conclusion, we report the photocatalytic activity of a triazine-based COF, **TRIPTA**, containing photoactive building blocks which facilitates both SET (single electron transfer) and reactive oxygen species ($O_2^{\bullet-}$ and/or $^1O_2$) generation in the absence and presence of oxygen, respectively, under visible light irradiation. Using the SET pathway, **TRIPTA** is found to efficiently catalyze the reductive debromination of phenacyl bromide via C−Br bond cleavage under visible light and N_2 atmosphere. In addition, **TRIPTA** exhibits remarkable conversion (>95%), high product selectivity, and good recyclability in the photooxidative benzylamine coupling reactions via ROS generation. Using this single-component model reaction, we further systematically investigated different-sized benzylamine substrates and compared the results with an

Table 3. Photocatalytic Efficiency of TRIPTA and Micro-COF-2 Towards Oxidative Self-coupling Reactions of Phenyl Benzylamine Derivatives

Entry	Substrate	Catalyst	Time (h)	Conversion (%)
1	(4-phenylbenzylamine, ~12.12 Å)	**TRIPTA**	1	~20
2	(4-phenylbenzylamine)	**Micro-COF-2**	1	>80
3	(4-(4-fluorophenyl)benzylamine, ~12.60 Å)	**TRIPTA**	1	~20
4	(4-(4-fluorophenyl)benzylamine)	**Micro-COF-2**	1	>80

analogous COF (**Micro-COF-2**) exhibiting a larger pore size. We observed a marked improvement in the conversion of larger-sized substates with the **Micro-COF-2**, thereby demonstrating the manifestation of angstrom-level pore size-selective photocatalysis with 2D-COFs. Taken together, our results open a new avenue for potential selective photocatalysis employing 2D-COFs based on judicious pore size design.

■ ASSOCIATED CONTENT

Ⓢ Supporting Information

The Supporting Information is available free of charge at https://pubs.acs.org/doi/10.1021/acsomega.4c06171.

Details of the synthesis, photocatalytic studies, and Supporting Figures S1−33 (PDF)

■ AUTHOR INFORMATION

Corresponding Author

Anindita Das − *Department of Chemistry, Southern Methodist University, Dallas, Texas 75275, United States;* ⓞ orcid.org/0000-0002-8855-8265; Email: aninditad@smu.edu

Authors

Melika Eshaghi Kenari − *Department of Chemistry, Southern Methodist University, Dallas, Texas 75275, United States*

Sayan Maiti − *Department of Chemistry, Southern Methodist University, Dallas, Texas 75275, United States*

Jianheng Ling − *Department of Chemistry and Chemical Biology, Cornell University, Ithaca, New York 14853, United States;* ⓞ orcid.org/0000-0002-9821-2188

Xena El-Shamy − *Department of Chemistry, Southern Methodist University, Dallas, Texas 75275, United States*

Hiren Bagga − *Department of Chemistry, Southern Methodist University, Dallas, Texas 75275, United States*

Matthew A. Addicoat − *School of Science and Technology, Nottingham Trent University, Nottingham NG11 8NS, United Kingdom;* ⓞ orcid.org/0000-0002-5406-7927

Phillip J. Milner − *Department of Chemistry and Chemical Biology, Cornell University, Ithaca, New York 14853, United States;* ⓞ orcid.org/0000-0002-2618-013X

Complete contact information is available at:
https://pubs.acs.org/10.1021/acsomega.4c06171

Author Contributions

#These authors contributed equally to this work.

Notes

The authors declare no competing financial interest.

■ REFERENCES

(1) Côté, A.; Benin, A.; Ockwig, N.; O'Keeffe, M.; Matzger, A.; Yaghi, O. Porous, Crystalline, Covalent Organic Frameworks. *Science* **2005**, *310*, 1166−1170.

(2) Largeron, M.; Neudorffer, A.; Fleury, M. B. Oxidation of Unactivated Primary Aliphatic Amines Catalyzed by an Electrogenerated 3,4-azaquinone Species: A Small-Molecule Mimic of Amine Oxidases. *Angew. Chem., Int. Ed.* **2003**, *42*, 1026−1029.

(3) Kramer, S.; Bennedsen, N. R.; Kegnaes, S. Porous Organic Polymers Containing Active Metal Centers as Catalysts for Synthetic Organic Chemistry. *ACS Catal.* **2018**, *8*, 6961−6982.

(4) Patel, A. R.; Patel, G.; Banerjee, S. Visible Light-Emitting Diode Light-Driven $Cu_{0.9}Fe_{0.1}$@RCAC-Catalyzed Highly Selective Aerobic Oxidation of Alcohols and Oxidative Azo-Coupling of Anilines: Tandem One Pot Oxidation-Condensation to Imidazoles and Imines. *ACS. Omega* **2019**, *4*, 22445−22455.

(5) Millet, A.; Cesana, P. T.; Sedillo, K.; Bird, M. J.; Schlau-Cohen, G. S.; Doyle, A. G.; MacMillan, D. W. C.; Scholes, G. D. *Acc. Chem. Res.* **2022**, *55*, 1423−1434.

(6) Zhang, X.; Zhang, J.; Hao, Z.; Han, Z.; Lin, J.; Lu, G.-L. Nickel Complexes Bearing N,N,O-Tridentate Salicylaldiminato Ligand: Efficient Catalysts for Imines Formation via Dehydrogenative Coupling of Primary Alcohols with Amines. *Organometallics.* **2021**, *40*, 3843−3853.

(7) Lepori, M.; Schmid, S.; Barham, J. P. Photoredox Catalysis Harvesting Multiple Photon or Electrochemical Energies. *Beilstein. J. Org. Chem.* **2023**, *19*, 1055−1145.

(8) Carson, W. P., II; Sarver, P. J.; Goudy, N. S.; MacMillan, D. W. C. Photoredox Catalysis-Enabled Sulfination of Alcohols and Bromides. *J. Am. Chem. Soc.* **2023**, *145*, 20767−20774.

(9) Lang, X.; Ma, W.; Chen, C.; Ji, H.; Zhao, J. Selective Aerobic Oxidation Mediated by TiO_2 Photocatalysis. *Acc. Chem. Res.* **2014**, *47*, 355−363.

(10) Zhang, L.; Shi, X.; Zhang, Z.; Kuchel, R. P.; Namivandi-Zangeneh, R.; Corrigan, N.; Jung, K.; Liang, K.; Boyer, C. Porphyrinic Zirconium Metal−Organic Frameworks (MOFs) as Heterogeneous Photocatalysts for PET-RAFT Polymerization and Stereolithography. *Angew. Chem., Int. Ed.* **2021**, *60*, 5489−5496.

(11) Huang, D.; Yan, X.; Yan, M.; Zeng, G.; Zhou, C.; Wan, J.; Cheng, M.; Xue, W. Graphitic Carbon Nitride-Based Heterojunction Photoactive Nanocomposites: Applications and Mechanism Insight. *ACS Appl. Mater. Interfaces* **2018**, *10*, 21035−21055.

(12) Mahmoud, N.; Awassa, J.; Toufaily, J.; Lebeau, B.; Daou, T. J.; Cormier, M.; Goddard, J.-P. Heterogeneous Photoredox Catalysis Based on Silica Mesoporous Material and Eosin Y: Impact of Material Support on Selectivity of Radical Cyclization. *Molecules* **2023**, *28*, 549.

(13) Parra-Ortiz, E.; Caselli, L.; Agnoletti, M.; Skoda, M. W. A.; Li, X.; Zhao, D.; Malmsten, M. Mesoporous Silica as a Matrix for Photocatalytic Titanium Dioxide Nanoparticles: Lipid Membrane Interactions. *Nanoscale* **2022**, *14*, 12297−12312.

(14) Yang, M.; Zhang, S.; Zhang, M.; Li, Z.; Liu, Y.; Liao, X.; Lu, M.; Li, S.; Lan, Y. Three-Motif Molecular Junction Type Covalent Organic Frameworks for Efficient Photocatalytic Aerobic Oxidation. *J. Am. Chem. Soc.* **2024**, *146*, 3396−3404.

(15) Li, Q.; Wang, J.; Zhang, Y.; Ricardez-Sandoval, L.; Bai, G.; Lan, X. Structural and Morphological Engineering of Benzothiadiazole-Based Covalent Organic Frameworks for Visible Light-Driven Oxidative Coupling of Amines. *ACS Appl. Mater. Interfaces* **2021**, *13*, 39291−39303.

(16) Wang, X.; Chen, L.; Chong, S. Y.; Little, M. A.; Wu, Y.; Zhu, W.-H.; Clowes, R.; Yan, Y.; Zwijnenburg, M. A.; Sprick, R. S.; Cooper, A. I. Sulfone-containing Covalent Organic Frameworks for Photo-

catalytic Hydrogen Evolution from Water. *Nat. Chem.* **2018**, *10*, 1180−1189.

(17) Zhang, T.; Zhang, G.; Chen, L. 2D Conjugated Covalent Organic Frameworks: Defined Synthesis and Tailor-Made Functions. *Acc. Chem. Res.* **2022**, *55*, 795−808.

(18) Meyer, C. D.; Joiner, C. S.; Stoddart, J. S. Gawronski, Template-directed Synthesis Employing Reversible Imine Bond Formation. *Chem. Soc. Rev.* **2007**, *36*, 1705−1723.

(19) (a) Pachfule, P.; Acharjya, A.; Roeser, J.; Sivasankaran, R. P.; Ye, M.-Y.; Bruckner, A.; Schmidt, J.; Thomas, A. Donor-acceptor covalent organic frameworks for visible light induced free radical polymerization. *Chem. Sci.* **2019**, *10*, 8316−8322. (b) Pachfule, P.; Acharjya, A.; Roeser, J.; Langenhahn, T.; Schwarze, M.; Schomacker, R.; Thomas, A.; Schmidt, J. Diacetylene Functionalized Covalent Organic Framework (COF) for Photocatalytic Hydrogen Generation. *J. Am. Chem. Soc.* **2018**, *140*, 1423−1427.

(20) Bhadra, M.; Kandambeth, S.; Sahoo, M. K.; Addicoat, M.; Balaraman, E.; Banerjee, R. Triazine Functionalized Porous Covalent Organic Framework for Photo-organocatalytic E−Z Isomerization of Olefins. *J. Am. Chem. Soc.* **2019**, *141*, 6152−6156.

(21) Wang, H.; Wang, H.; Wang, Z.; Tang, L.; Zeng, G.; Xu, P.; Chen, M.; Xiong, T.; Zhou, C.; Li, X.; Huang, D.; Zhu, Y.; Wang, Z.; Tang, J. Covalent Organic Framework Photocatalysts: Structures and Applications. *J. Chem. Soc. Rev.* **2020**, *49*, 4135−4165.

(22) Li, Z.; Zhi, Y.; Shao, P.; Xia, H.; Li, G.; Feng, X.; Chen, X.; Shi, Z.; Liu, X. Covalent Organic Framework as an Efficient, Metal-Free, Heterogeneous Photocatalyst for Organic Transformations under Visible Light. *Appl. Catal., B* **2019**, *245*, 334−342.

(23) Wu, C.; Li, X.; Li, T.; Shao, M.; Niu, L.; Lu, X.; Kan, J.; Geng, Y.; Dong, Y. Natural Sunlight Photocatalytic Synthesis of Benzoxazole-Bridged Covalent Organic Framework for Photocatalysis. *J. Am. Chem. Soc.* **2022**, *144*, 18750−18755.

(24) Traxler, M.; Gisbertz, S.; Pachfule, P.; Schmidt, J.; Roeser, J.; Reischauer, S.; Rabeah, J.; Pieber, B.; Thomas, A. Acridine-Functionalized Covalent Organic Frameworks (COFs) as Photocatalysts for Metallaphotocatalytic C−N Cross-Coupling. *Angew. Chem., Int. Ed.* **2022**, *61*, No. e2021177.

(25) Mu, Z.; Zhu, Y.; Li, B.; Dong, A.; Wang, B.; Feng, X. Covalent Organic Frameworks with Record Pore Apertures. *J. Am. Chem. Soc.* **2022**, *144*, 5145−5154.

(26) Huo, J.; Aguilera-Sigalat, J.; El-Hankari, S.; Bradshaw, D. Magnetic MOF Microreactors for Recyclable Size-Selective Biocatalysis. *Chem. Sci.* **2015**, *6*, 1938−1943.

(27) Li, W.; Zhang, Y.; Xu, Z.; Meng, Q.; Fan, Z.; Ye, S.; Zhang, G. Assembly of MOF Microcapsules with Size-Selective Permeability on Cell Walls. *Angew. Chem., Int. Ed.* **2016**, *55*, 955−959.

(28) Zhang, X.; Jing, L.; Wei, L.; Zhang, F.; Yang, H. Semipermeable Organic−Inorganic Hybrid Microreactors for Highly Efficient and Size-Selective Asymmetric Catalysis. *ACS Catal.* **2017**, *7*, 6711−6718.

(29) González-Muñoz, D.; Casado-Sánchez, A.; del Hierro, I.; Gómez-Ruiz, S.; Cabrera, S.; Alemán, J. Size-Selective Mesoporous Silica-based Pt(II) Complex as Efficient and Reusable Photocatalytic Material. *J. Catal.* **2019**, *373*, 374−383.

(30) Goswami, R.; Bankar, B.; Rajput, S.; Seal, N.; Pillai, R.; Biradar, A.; Neogi, S. In situ Fabricated MOF-Cellulose Composite as an Advanced ROS Deactivator Convertor: Fluoroswitchable Bi-Phasic Tweezers for Free Chlorine Detoxification and Size-Exclusive Catalytic Insertion of Aqueous H_2O_2. *J. Mater. Chem.* **2022**, *10*, 4316−4332.

(31) Das, S. K.; Roy, S.; Das, A.; Chowdhury, A.; Chatterjee, N.; Bhaumik, A. A Conjugated 2D Covalent Organic Framework as a Drug Delivery Vehicle Towards Triple Negative Breast Cancer Malignancy. *Nanoscale Adv.* **2022**, *4*, 2313−2320.

(32) Gao, S.; Guo, L.; Wan, W.; Li, Z.; Wang, H.; Luo, S.; Wang, J. Covalent Organic Framework Membrane with Angstrom Discrimination in Pore Size for Highly Permselective Ionic Liquid Nanofiltration. *ACS Sustainable Chem. Eng.* **2023**, *11*, 15910−15918.

(33) An, S.; Zhu, X.; He, Y.; Yang, L.; Wang, H.; Jin, S.; Hu, J.; Liu, H. Porosity Modulation in Two-Dimensional Covalent Organic Frameworks Leads to Enhanced Iodine Adsorption Performance. *Ind. Eng. Chem. Res.* **2019**, *58*, 10495−10502.

(34) Gomes, R.; Bhaumik, A. A New Triazine Functionalized Luminescent Covalent Organic Framework for Nitroaromatic Sensing and CO_2 Storage. *RSC Adv.* **2016**, *6*, 28047.

(35) Wang, L.-J.; Dong, P.-Y.; Zhang, G.; Zhang, F.-M. Review and Perspectives of β-Keto-enamine-Based Covalent Organic Framework for Photocatalytic Hydrogen Evolution. *Energy Fuels* **2023**, *37* (9), 6323−6347.

(36) Koner, K.; Mohata, S.; Ogaeri, Y.; Nishiyama, Y.; Addicoat, M. A.; Banerjee, R. Enhancing the Crystallinity of Keto-enamine-Linked Covalent Organic Frameworks through an in situ Protection-Deprotection Strategy. *Angew. Chem., Int. Ed.* **2024**, *63*, No. e202316873.

(37) Li, M.; Yang, Q.; Fan, L.; Dai, X.; Kang, Z.; Wang, R.; Sun, D. An Ultrastable Bifunctional Electrocatalyst Derived from a Co^{2+}-Anchored Covalent−Organic Framework for High-Efficiency ORR/OER and Rechargeable Zinc−Air Battery. *ACS Appl. Mater. Interfaces* **2023**, *15*, 39448−39460.

(38) Das, S. K.; Kumar, G.; Das, M.; Dey, R. S. A 2D Covalent Organic Framework as a Metal-Free Electrode Towards Electrochemical Oxygen Reduction Reaction. *Materials Today: Proceedings* **2022**, *57*, 228−233.

(39) Singh, N.; Yadav, D.; Mulay, S.; Kim, J.; Park, N.; Baeg, J. Band Gap Engineering in Solvochromic 2D Covalent Organic Framework Photocatalysts for Visible Light-Driven Enhanced Solar Fuel Production from Carbon Dioxide. *ACS Appl. Mater. Interfaces.* **2021**, *13*, 14122−14131.

(40) Wang, W.; Huang, D.; Zheng, W.; Zhao, X.; He, K.; Pang, H.; Xiang, Y. Construction of Amide-Linked Covalent Organic Frameworks by N-Heterocyclic Carbene-Mediated Selective Oxidation for Photocatalytic Dehalogenation. *Chem. Mater.* **2023**, *35*, 7154−7163.

(41) Wang, Z.; Qian, J.; Wang, S.; Wen, Z.; Xiao, S.; Hu, H.; Gao, Y. Benzodiazole-Based Covalent Organic Frameworks for Enhanced Photocatalytic Dehalogenation of Phenacyl Bromide Derivatives. *Polymers* **2024**, *16*, 2578.

(42) Li, Z.; Zhi, Y.; Shao, P.; Xia, H.; Li, G.; Feng, X.; Chen, X.; Shi, Z.; Liu, X. Covalent Organic Framework as an Efficient, Metal-Free, Heterogeneous Photocatalyst for Organic Transformations Under Visible Light. *Appl. Catal. B: Environ.* **2019**, *245*, 334−342.

(43) Liu, H.; Li, C.; Li, H.; Ren, Y.; Chen, J.; Tang, J.; Yang, Q. Structural Engineering of Two-Dimensional Covalent Organic Frameworks for Visible-Light-Driven Organic Transformations. *ACS Appl. Mater. Interfaces.* **2020**, *12*, 20354−20365.

(44) Shan, H.; Cai, D.; Zhang, X.; Zhu, Q.; Qin, P.; Baeyens, J. Donor-Acceptor Type Two-Dimensional Porphyrin-based Covalent Organic Framework for Visible-Light-Driven Heterogeneous Photocatalysis. *Chem. Eng. J.* **2022**, *432*, No. 134288.

(45) Goel, B.; Vyas, V.; Tripathi, N.; Kumar Singh, A.; Menezes, P. W.; Indra, A.; Jain, S. K. Amidation of Aldehydes with Amines under Mild Conditions Using Metal-Organic Framework Derived NiO@Ni Mott-Schottky Catalyst. *ChemCatChem* **2020**, *12*, 5743−5749.

(46) Li, X.; Hao, H.; Lang, X. Thiazolo[5,4-d]thiazole Linked Conjugated Microporous Polymer Photocatalysis for Selective Aerobic Oxidation of Amines. *J. Colloid Interface Sci.* **2021**, *593*, 380−389.

(47) Wu, S.; Zhang, Y.-F.; Ding, H.; Li, X.; Lang, X. Hydrazone-linked 2D Porphyrinic Covalent Organic Framework Photocatalysis for Visible Light-Driven Aerobic Oxidation of Amines to Imines. *J. Colloid Interface Sci.* **2022**, *610*, 446−454.

(48) Li, M.-H.; Yang, Z.; Li, Z.; Wu, J.-R.; Yang, B.; Yang, Y.-W. Construction of Hydrazone-Linked Macrocycle-Enriched Covalent Organic Frameworks for Highly Efficient Photocatalysis. *Chem. Mater.* **2022**, *34*, 5726−5739.

(49) Li, S.; Li, L.; Li, Y.; Dai, L.; Liu, G.; Liu, Y.; Li, J.; Lv, J.; Li, P.; Wang, B. Fully Conjugated Donor−Acceptor Covalent Organic Frameworks for Photocatalytic Oxidative Amine Coupling and Thioamide Cyclization. *ACS Catal.* **2020**, *10*, 8717−8726.

(50) Schümperli, M. T.; Hammond, C.; Hermans, I. Developments in the Aerobic Oxidation of Amines. *ACS Catal.* **2012**, *2*, 1108−1117.

(51) Largeron, M. Protocols for the Catalytic Oxidation of Primary Amines to Imines. *Eur. J. Org. Chem.* **2013**, *2013*, 5225−5235.

(52) Ma, J.; Miao, T. J.; Tang, J. Charge Carrier Dynamics and Reaction Intermediates in Heterogeneous Photocatalysis by Time-Resolved Spectroscopies. *Chem. Soc. Rev.* **2022**, *51*, 5777−5794.